

Channel Estimation for Residual Self-Interference in Full-Duplex Amplify-and-Forward Two-Way Relays

Xiaofeng Li, Cihan Tepedelenlioğlu, *Member, IEEE*, and Habib Şenol, *Member, IEEE*

Abstract—Training schemes for full duplex two-way relays are investigated. We propose a novel one-block training scheme with a maximum likelihood estimator to estimate the channels between the nodes as well as the residual self-interference (RSI) channel simultaneously. A quasi-Newton algorithm is used to solve the estimator. As a baseline, a multi-block training scheme is also considered. The Cramer–Rao bounds of the one-block and multi-block training schemes are derived. By using the Szegő’s theorem about Toeplitz matrices, we analyze how the channel parameters and transmit powers affect the Fisher information. We show analytically that exploiting the structure arising from the RSI channel increases its Fisher information. Numerical results show the benefits of estimating the RSI channel.

Index Terms—Channel estimation, residual self-interference, full-duplex relay, asymptotic Toeplitz matrix, two-way relay.

I. INTRODUCTION

AS the demand in wireless bandwidth resources grows, efficient utilization of spectrum has become more urgent. In-band full duplex radio has drawn great attention from both the industry and academia, due to its potential to improve spectral efficiency. Recent progresses achieved in self-interference cancellation has made the implementation of in-band full duplex possible [1], which has the potential to support the demands on the fifth generation wireless communication systems [2]. Meanwhile, relaying, another popular technology that has a part to play in the next generation wireless networks, is able to provide not only additional throughput, but also improved coverage. Compared with traditional one-way relays, both full-duplex and two-way relay with analog network coding can individually double the bandwidth theoretically, which leads to a potential improvement in spectral efficiency by a factor of 4. Though the residual self-interference and the synchronization problems from the two techniques respectively reduce the efficiency, it is not enough to cancel the gain. Thus, the integration of in-band full duplex and two-way relay has large potential to improve spectral efficiency.

As mentioned above, self-interference cancellation is an enabler for full duplex one-way relay networks. Thus many

recent studies are conducted to approach the issue of self-interference cancellation from diverse aspects, including propagation domain, time domain and spatial domain approaches [3]. In propagation domain, physical isolation and directional antennas are used. Least squares channel estimate for full duplex is considered in [4]. Reference [5] proposes a maximum likelihood channel estimator in which the relay estimates the self-interference channel as well as the channel from the source to the relay. An analog self-interference cancellation method using effective channel parameters obtained from channel estimation is used in [6]. In spatial domain approaches, multiple antennas for transmitting and receiving are adopted at the relay to exploit the potential of extra degrees of freedom for interference cancellation. In [7], linear precoders and decoders are designed at the relay, which aim to minimize the power of self-interference. Reference [8] designs a pre-coding matrix which suppresses the self-interference and maximizes the sum-rate jointly in a full duplex multiuser MIMO system. Similarly, [9] aims to maximize the end-to-end signal-to-noise ratio (SNR) as well as suppressing the self-interference by jointly optimizing pre-coding matrices at the relay in a two-way relay system. The combination of these approaches can provide a high attenuation of the self-interference power. However, the RSI is still quite high compared to the desired received signal, and does not yield good performance when treated as noise. Kim and Paulraj [10] assume the RSI is 10 dB higher than the received signal and causes inter-symbol interference (ISI) in amplify-and-forward relays due to feedback. References [3], [11], and [12] also report that the power of RSI is about 30 dB higher than the noise floor.

The existence of RSI has also been addressed in the literature [3], [7], [10]–[13]. One reason for the presence of RSI is due to the limitation of time domain cancellation which suffers from estimation error in the pre-stage [13]. In full duplex relay systems, there is a pre-stage before the transmission of training and data phases for self-interference cancellation. In the pre-stage, the relay estimates the self-interference channel and uses the estimates to cancel the self-interference in RF before analog to digital conversion [5]. The pre-stage estimation error is caused by noise, and time variation of the self-interference channel. The self-interference channel consists of a line-of-sight part and a diffuse path part [11], [13]. The line of sight part almost remains the same for a relatively long interval and dominates the self-interference. Thus using the pre-stage estimates to cancel the self-interference significantly reduces the power of self-interference. However, the diffuse part changes more often and the estimates are not

Manuscript received June 4, 2016; revised January 6, 2017; accepted April 27, 2017. Date of publication May 18, 2017; date of current version August 10, 2017. The associate editor coordinating the review of this paper and approving it for publication was Y. Xin. (*Corresponding author: Xiaofeng Li.*)

X. Li and C. Tepedelenlioğlu are with the Department of Electrical, Computer and Energy Engineering, Arizona State University, Tempe, AZ 85287 USA (e-mail: xiaofen2@asu.edu; cihan@asu.edu).

H. Şenol is with the Department of Computer Engineering, Faculty of Engineering and Natural Sciences, Kadir Has University, 34083 Istanbul, Turkey (e-mail: hsenol@khas.edu.tr).

Color versions of one or more of the figures in this paper are available online at <http://ieeexplore.ieee.org>.

Digital Object Identifier 10.1109/TWC.2017.2704123

accurate for it over time. This part can also be seen as an estimation error and results in RSI. The second reason for RSI is seen from the spatial domain when using multiple antennas for both transmitting and receiving at the relay. Reference [7] investigates how to design pre-coding matrices to mitigate the self-interference and all the degrees of freedom (DoF) offered by antennas are used for the purpose of interference cancellation. However, when multiple antennas are used, beamforming for maximizing the transmission rate can also be considered. Reference [9] jointly designs pre-coding matrices minimizing the self-interference while maximizing the rate. Since part of the DoF is used for improving the rate, the effort of mitigating the self-interference is not as good as the one which uses all the DoF, which also results in RSI. Thus, there is a trade-off between maximizing the rate and suppressing the self-interference.

Many previous works consider the full-duplex relay system in the presence of RSI. For one-way relays, some studies analyze the system performance without considering the cancellation of the RSI [10], [12], [14], [15]. The outage probability of amplify-and-forward full duplex relay is investigated in [10]. Reference [12] analyzes the RSI power after null-space suppression. The error and diversity performances is analyzed in [14]. The capacity of full duplex relays is studied in [15]. While reference [16] considers the RSI cancellation by estimating the RSI channel in traditional one-way relays, it does not address two-way relays, and also lacks the asymptotic Cramer-Rao bound (CRB) analysis provided herein.

Several papers consider the full duplex two-way relays [9], [17]–[19]. Reference [17] compares the achievable rates of full duplex relay and half duplex relay. The effect of channel estimation error and suppression of the self-interference are investigated in [18] and [19]. Precoder matrix design for suppressing the self-interference and performance analysis of end-to-end SNR are addressed in [9] in the absence of RSI. However, the effect of RSI at the two sources are not considered. The method to conduct channel estimation in full duplex relays, which is very different from the half duplex scenario of e.g. [20], [21], is not considered in the literature either.

In this paper, we focus on analyzing the channel estimation problem in a two-way relay system with a full-duplex relay helping to exchange data between two full duplex capable devices in the presence of RSI. Though the channel estimation can be done by making the training phase working in half duplex mode, it is more spectrally efficient to estimate the channels in full duplex mode. Moreover, the RSI from the relay makes the overall end-to-end channel an ISI channel [10], [12]. To improve the performance, the estimation and equalization of the ISI channel parameters are needed. Thus we estimate the RSI in the destination node to enable cancellation of the interference of the system further, through equalization. We propose a novel one-block training scheme and two baseline methods to estimate the RSI channel at both sources in an amplify-and-forward two-way relay system for the first time in the literature. The one-block training scheme uses one transmission block to keep

the relay protocol consistent with the data phase. An ML estimator is derived to estimate the RSI channel as well as the individual channels. A popular quasi-Newton method, the Broyden-Fletcher-Goldfarb-Shanno (BFGS) algorithm [22], is used to numerically solve the ML estimator. Zero-forcing estimation is used for initialization values to improve the accuracy and reduce the complexity of the ML estimator.

As a baseline, we also propose a multi-block training scheme in which the traditional least squares (LS) channel estimation method is used. In addition, the cross-correlation method for estimating the ISI channel is also considered for comparison. In the former, a half duplex transmission protocol is needed in the training phase to make the received signal linear in the RSI channel. The two baseline approaches estimate the same channel parameters as the one-block scheme does. The CRBs for both training schemes are derived respectively to assess the fundamental limits of each training scheme.

Our contributions are summarized as follows:

1. We propose a one-block training scheme with an ML estimator. The BFGS method combined with zero-forcing initialization are used to compute the estimator efficiently. A simple and intuitive multi-block training scheme is proposed and serves as a baseline. LS estimator is used in this case. The cross-correlation method for ISI channel estimation is also applied for comparison.

2. CRBs for different training schemes are derived and compared. We analyze how the channel parameters and transmit powers affect the Fisher information for large training length by using the Szegő's theorem about the asymptotic properties of Toeplitz matrices. We also show analytically that the Fisher information with exploiting the channel structure arising from the full duplex model is greater than the Fisher information which does not take the structure into account for the RSI channel.

3. To show the importance of estimating the RSI channel and canceling the RSI, matched filter detector and Viterbi equalizer are implemented. The former uses channel state information (CSI) of the cascaded channel only, while the latter uses all the CSI including the RSI channel. The Viterbi equalizer outperforms the matched filter in bit error rate (BER) comparisons in the whitened noise case. We also consider the BER with whitened noise which requires the CSI of RSI channel for noise whitening, and compare it favorably with the unwhitened noise case.

The rest of the paper is organized as the follows: Section II describes the system model of a full duplex two-way relay system. Section III proposes the one-block training scheme. Section IV provides the two baselines for comparison. The CRBs for different training schemes and channel structure assumptions are derived and the Fisher information is analyzed in Section V. Section VI shows the simulation results and Section VII concludes the paper.

II. SYSTEM MODEL

We consider a system with two sources and a relay in between, with no direct link, as shown in Figure 1. The sources and the relay are equipped with two antennas, one

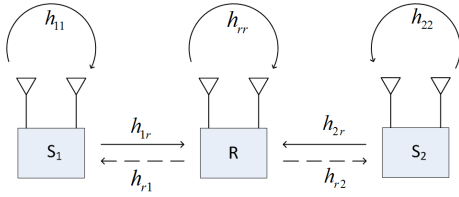


Fig. 1. Two-way relay in full duplex mode.

servicing as a receive antenna while the other one a transmit antenna. The amplify-and-forward scheme is adopted at the relay. To operate this scheme in the full duplex mode, the relay receives the current symbols while it amplifies and forwards the previously received symbols. The channel coefficients between source 1 and the relay, and source 2 and the relay are h_{1r} and h_{2r} , respectively. The reverse channels between the relay and the two sources are h_{r1} and h_{r2} . Without loss of generality, we assume the forward and reverse channels between a source and the relay are different (i.e. we do not assume the channels are reciprocal, which also could be handled with some modifications). These channels between nodes are referred to individual channels in this paper while the product of two individual channels are cascaded channels. The four channels above are complex Gaussian, independent, with zero means and unit variance. They are also assumed to be time invariant across multiple blocks. The noise at both sources and the relay are assumed to be complex Gaussian with zero mean and variance σ_v^2 . Perfect synchronization is assumed in our system. The methods for synchronization in half duplex can be extended to full duplex [23] and used in conjunction without methods.

In our system model, the relay estimates the self-interference channel in the pre-stage and uses the estimates to cancel the self-interference in the following transmission as mentioned in Section I. The RSI channel which is due to the pre-stage estimation error can be modeled as a flat fading channel [7], [10]. Let h_{rr} , h_{11} , h_{22} be the RSI channel between the two antennas at the relay and source nodes. They are with zero means and variance σ_{rr}^2 , σ_{11}^2 , σ_{22}^2 respectively which capture the inaccuracy in self-interference cancellation in the pre-stage. The RSI power, which is related to the transmit power of the relay, is not small enough to be treated as noise, and often higher than the desired signal power. Moreover, it makes the overall end-to-end channel an ISI channel in the AF relay even when the channels on all links are flat fading. The CSI of the RSI channel is needed for equalizers to alleviate the ISI at the receiver.

III. ONE-BLOCK TRAINING SCHEME

In this section, we propose the one-block training scheme for full duplex transmission training and compare it with the multi-block training scheme which is proposed in the following section. The one-block scheme consists of only one block consisting of N symbols during training and the multi-block scheme consists of four blocks that have a total of N symbols. One block in our scheme means one transmission phase that

either the source or the relay node transmits its training sequence without changing the transmission protocol. In the one-block scheme, we consider the transmission from source 1 to source 2 : source 1 transmits its training sequence (and the relay forwards) for the whole training. No nodes change their training protocols and thus this training scheme is considered as one block. In contrast, in the multi-block scheme, in the first block source 1 transmits its training sequence. Then in the second block source 1 stops and the relay transmits what it received in the previous block. In the third block the relay transmits its own training data and in the fourth block the relay transmits what it received in the third block. Hence the transmission protocol changes multiple times during training. Each time it changes is a different block during training. The overhead due to training, which is the total training length, is one block length for the one-block scheme and four blocks for the multi-block scheme. In the comparison of the two schemes, we fix the training overhead, which leads to different block lengths for the two schemes. The one-block scheme has N symbols per block, and the multi-block scheme has $N/4$ symbols per block that totals N symbols during training.

A. The Training Phase

In the training phase, we extend to full duplex the two time slot relaying protocol for half duplex in which two sources transmit their signals to the relay simultaneously in the first time slot and the relay broadcasts its received signal in the second time slot. In full duplex mode, the transmission of the two sources and the broadcast of the relay happens in the same symbol interval. The relay receives the current signal while continuing to transmit its received signal in the previous symbol interval. For the purpose of training, the relay adds its own training sequence to its received signal, scales the processed signal to satisfy the power constraint, then it transmits the scaled signal. The sources also transmit and receive together. At symbol interval n , the relay receives

$$y_r[n] = h_{1r}x_1[n] + h_{2r}x_2[n] + h_{rr}t_r[n] + v_r[n], \quad (1)$$

where $x_1[n]$ and $x_2[n]$ are the training sequences sent by source 1 and source 2 respectively where $|x_1[n]|^2 = |x_2[n]|^2 = P_s$, $t_r[n]$ is the transmit signal of the relay and this term is the RSI due to the broadcast of the previous received signal at the relay in the previous time slot, and $v_r[n] \sim \mathcal{CN}(0, \sigma_v^2)$. The relay adds its own training sequence $x_r[n]$ satisfying $|x_r[n]|^2 = P_s$ and scales the processed signal. Following [10], we assume there is a one-symbol delay for the relay to forward its received symbols, which is due to the self interference cancellation processing. The transmit signal of the relay therefore is

$$t_r[n] = \alpha(y_r[n-1] + x_r[n-1]), \quad (2)$$

where α is a power scaling factor used to satisfy the power constraint at the relay. At source 1, the received symbol at

time n is

$$y_1[n] = h_{r1}t_r[n] + h_{11}x_1[n] + v_1[n] \quad (3)$$

$$= \sum_{k=1}^{\infty} \theta^{(k-1)} (px_1[n-k] + qx_2[n-k] + dx_r[n-k]) \\ + h_{11}x_1[n] + \sum_{k=1}^{\infty} d\theta^{(k-1)}v_r[n-k] + v_1[n], \quad (4)$$

where we define $p := ah_{r1}h_{1r}$, $q := ah_{r1}h_{2r}$, $d := ah_{r1}$, and $\theta := ah_{rr}$ for simplicity. The recursive form of (4) is obtained by substituting (1) and (2) in (3). Due to the feedback in the self-interference link θ at the relay, the overall channel in (4) is a single pole infinite impulse response (IIR) channel which causes ISI. Moreover, the effective noise is colored with correlations that depend on the pole. The impulse response for $x_1[n]$ is $p[k] := p\theta^{k-1}$, and for $x_2[n]$ is $q[k] = q\theta^{k-1}$, $k = 1, 2, \dots$.

The power scaling factor α is chosen to keep the system stable and guarantee finite relay transmit power. The relay transmit power is calculated as

$$\begin{aligned} & \mathbb{E}[t_r[n]t_r^*[n]] \\ &= \alpha^2 \sum_{k=1}^{\infty} (\alpha^2|h_{rr}|^2)^{(k-1)} (P_s|h_{1r}|^2 + P_s|h_{2r}|^2 + P_s + \sigma_v^2) \\ &= \alpha^2 \frac{P_s|h_{1r}|^2 + P_s|h_{2r}|^2 + P_s}{1 - \alpha^2|h_{rr}|^2}. \end{aligned} \quad (5)$$

By solving $\mathbb{E}[t_r[n]t_r^*[n]] \leq P_r$, α should satisfy $\alpha^2 < 1/|h_{rr}|^2$ [24]. However, in a channel estimation scenario, the instantaneous CSI is not available. We can choose α to satisfy a long term condition which is $\alpha^2 < 1/\mathbb{E}[|h_{rr}|^2] = 1/\sigma_{rr}^2$, and σ_{rr} can be obtained at the pre-stage. Therefore, we choose the power scaling factor as

$$\alpha^2 = \frac{P_r}{3P_s + P_r\sigma_{rr}^2 + \sigma_v^2}, \quad (6)$$

where P_r is the transmit power of the relay. With this power scaling factor, the average RSI power is $P_r\sigma_{rr}^2$. We can also setup a fixed, pre-defined gain margin to prevent the instantaneous $|h_{rr}|$ value from exceeding the constraint.

We define L as the effective length of the overall channel impulse response in where most of the energy, e.g. 99%, is contained [10]. Thus, a block based transmission can be adopted with a guard time of L symbol intervals in which the sources keep silent to avoid inter-block interference. Without loss of generality, we assume the block length N is far greater than L , so the rate loss due to the guard time is negligible. We can now rewrite (4) for block transmission. For the m th block, the n th received symbol is

$$\begin{aligned} y_1^{(m)}[n] &= \sum_{k=1}^{\infty} \theta^{(k-1)} (px_1[u+n-k] + qx_2[u+n-k] \\ &\quad + dx_r[u+n-k]) + h_{11}x_1[u+n] \\ &\quad + \sum_{k=1}^{\infty} d\theta^{(k-1)}v_r[u+n-k] + v_1[u+n], \end{aligned} \quad (7)$$

where $u = (m-1)(N+L)$, for $n = 0, 1, 2, \dots, N+L$, and $m = 1, 2, \dots$, and $x_1[n] = x_2[n] = x_r[n] = 0$ for $n = N+1, \dots, N+L$. With the last L symbols of every block being zero, there is no inter-block interference, which allow us to drop the block index henceforth.

To write the output of the system in vector form, we relate $\mathbf{x}_1 = [x_1[0], \dots, x_1[N-1]]^T$, $\mathbf{x}_2 = [x_2[0], \dots, x_2[N-1]]^T$, $\mathbf{x}_r = [x_r[0], \dots, x_r[N-1]]^T$, and $\mathbf{y}_1 = [y_1[1], \dots, y_1[N]]^T$ as follows:

$$\mathbf{y}_1 = p\mathbf{H}_\theta\mathbf{x}_1 + q\mathbf{H}_\theta\mathbf{x}_2 + d\mathbf{H}_\theta\mathbf{x}_r + d\mathbf{H}_\theta\mathbf{v}_r + h_{11}\mathbf{J}^u\mathbf{x}_1 + \mathbf{v}_1, \quad (8)$$

where \mathbf{J}^u is an $N \times N$ upshift matrix given by a Toeplitz matrix with the first column $[0, 0, \dots, 0]^T$ and the first row $[0, 1, 0, \dots, 0]$, and \mathbf{H}_θ is an $N \times N$ Toeplitz matrix with the first row $[1, 0, \dots, 0]$ and the first column $[1, \theta, \theta^2, \dots, \theta^{L-1}, 0, \dots, 0]^T$. Note that the last L guard time symbols of every block are discarded so that the lengths of the input and output vector are N .

The data phase uses the same protocol as the training phase. The only difference is the relay does not add its own signal when forwarding its received overlapped signal. The received data signal at source 1 is

$$\mathbf{y}_{1d} = p\mathbf{H}_\theta\mathbf{x}_{1d} + q\mathbf{H}_\theta\mathbf{x}_{2d} + d\mathbf{H}_\theta\mathbf{v}_{rd} + h_{11}\mathbf{J}^u\mathbf{x}_{1d} + \mathbf{v}_{1d}, \quad (9)$$

where $\mathbb{E}[|x_{1d}[n]|^2] = \mathbb{E}[|x_{2d}[n]|^2] = P_s$.

B. Maximum Likelihood Estimator

In this section, we derive the ML estimator for source 1 but it's similar for source 2 due to symmetry. For data detection and better performance, not only the two cascaded channels $h_{r1}h_{1r}$ and $h_{r1}h_{2r}$ are needed, but also the colored noise needs be whitened. The whitening of the noise requires source 1 to have the knowledge of the RSI channel at the relay and the individual channels, either via relay feedback or estimating them by itself. Due to the impracticality of the feedback channel, source 1 will estimate the RSI channel as well as the individual channels in our approach. Though knowing the cascaded channels is enough to detect the data, more benefits can be obtained by using the knowledge of individual channels [25]. Estimating the individual channels needs the relay to send its own training sequence.

From (8), channel parameters p , q , θ , d , and h_{11} are complex unknown parameters to be estimated. We define $\boldsymbol{\omega} = [p_x, p_y, q_x, q_y, \theta_x, \theta_y, d_x, d_y, h_{11x}, h_{11y}]^T$ as the parameter vector, where p_x and p_y are the real and imaginary part for p respectively and similar to the other complex parameters. We separate the real and imaginary parts because BFGS algorithm optimizes with respect to real parameters. Given $\boldsymbol{\omega}$, the mean and the covariance matrix of \mathbf{y}_1 are given by

$$\boldsymbol{\mu} = \mathbb{E}[\mathbf{y}_1] = p\mathbf{H}_\theta\mathbf{x}_1 + q\mathbf{H}_\theta\mathbf{x}_2 + d\mathbf{H}_\theta\mathbf{x}_r + h_{11}\mathbf{J}^u\mathbf{x}_1, \quad (10)$$

$$\mathbf{C} = |d|^2\sigma_v^2\mathbf{H}_\theta\mathbf{H}_\theta^H + \sigma_v^2\mathbf{I}_N. \quad (11)$$

Thus, the likelihood function of \mathbf{y}_1 is

$$p(\mathbf{y}_1; \boldsymbol{\omega}) = \frac{1}{\pi^N |\mathbf{C}|} \exp\left(-(\mathbf{y}_1 - \boldsymbol{\mu})^H \mathbf{C}^{-1} (\mathbf{y}_1 - \boldsymbol{\mu})\right),$$

where $|C|$ denotes the determinant of matrix C . The corresponding log-likelihood function is

$$\log p(\mathbf{y}_1; \boldsymbol{\omega}) = -N \log \pi - \log |C| - (\mathbf{y}_1 - \boldsymbol{\mu})^H C^{-1} (\mathbf{y}_1 - \boldsymbol{\mu}). \quad (12)$$

Maximizing the likelihood function is equivalent to minimizing the last two terms in (12). Let $f(\boldsymbol{\omega})$ denote our objective function, then we have

$$f(\boldsymbol{\omega}) = \log |C| + (\mathbf{y}_1 - \boldsymbol{\mu})^H C^{-1} (\mathbf{y}_1 - \boldsymbol{\mu}). \quad (13)$$

Thus the ML estimator is given by

$$\hat{\boldsymbol{\omega}} = \arg \min_{\boldsymbol{\omega}} f(\boldsymbol{\omega}). \quad (14)$$

The objective function is not jointly convex with respect to $\boldsymbol{\omega}$. To solve the problem numerically, we use the BFGS algorithm, which is a popular quasi-Newton method. The BFGS is guaranteed to converge to a local minimum no matter whether the objective function is convex or not [26]. Also, the BFGS often needs less steps to converge than the gradient descent method [22], and thus is more efficient.

The parameters in $\boldsymbol{\omega}$ are optimized with different steps rather than optimizing $\boldsymbol{\omega}$ as a whole since they have different scales. For example d_x and θ_x are related to the relay-to-source channel and the RSI channel receptively. The gain of RSI channel is far smaller than that of the channel between nodes. So it is better to use different stepsizes when optimizing them. The algorithm takes the estimates of the real and imaginary part as the initial values. Due to the non-convexity, the algorithm might be trapped in a local minimum that is far from the optimal solution. Thus, it is necessary to initialize properly, which will be discussed in the following subsection. Backtracking line search is used to determinate the stepsize in the update process. The gradients needed in the BFGS method are derived in Appendix A. They are taken with respect to real parameters which are the elements in $\boldsymbol{\omega}$.

Our ML approach can be extended to frequency selective fading. In that case, the overall channel is a product of three Toeplitz matrices caused by the source-to-relay channel, RSI channel and relay-source channel. We can use Szegő's theorem for Toeplitz matrices which is explained in detail in Section V.C to approximate the overall channel matrix to a Toeplitz matrix. According to the theorem, when the training length is large, the product of two Toeplitz matrices is still a Toeplitz matrix and the elements of the product can be determined by the elements of the two matrices. Thus our ML method can be applied to estimate the overall channel even in the frequency selective setup.

C. Initialization

We use zero-forcing (ZF) estimation method to initialize the BFGS method. The first five received symbols at source 1 are taken to estimate h_{11} , p , q , d , and θ . The five symbols used are

$$y_1[0] = h_{11}x_1[0] + v_1[0], \quad (15)$$

$$y_1[i] = \sum_{k=1}^i \theta^{k-1} (px_1[i-k] + qx_2[i-k] + dx_r[i-k]) + h_{11}x_1[i] + \sum_{k=1}^i d\theta^{k-1}v_r[i-k] + v_1[i]. \quad (16)$$

We obtain the estimate of h_{11} first by the following.

$$\hat{h}_{11} = \frac{y_1[0]}{x_1[0]}. \quad (17)$$

Define $\tilde{y}_1[i] = y_1[i] - \hat{h}_{11}x_1[i]$ and we may design the training symbols to make it easier to estimate the other four parameters. Let $x_1[0] = x_1[1]$, $x_2[0] = x_2[1]$, and $x_r[0] = x_r[1]$. With ZF method, the noise is ignored. We can estimate θ by using $\tilde{y}_1[1]$ and $\tilde{y}_1[2]$:

$$\hat{\theta} = \frac{\tilde{y}_1[2] - \tilde{y}_1[1]}{y_1[1]}. \quad (18)$$

Let $\tilde{y}'_1[1] = \tilde{y}_1[1] - \hat{\theta}y_1[i-1]$ for $i = 2, 3, 4$. Then, the estimator of p , q , and d are

$$\begin{bmatrix} \hat{p} \\ \hat{q} \\ \hat{d} \end{bmatrix} = \begin{bmatrix} x_1[1] & x_2[1] & x_r[1] \\ x_1[2] & x_2[2] & x_r[2] \\ x_1[3] & x_2[3] & x_r[3] \end{bmatrix}^{-1} \begin{bmatrix} \tilde{y}'_1[2] \\ \tilde{y}'_1[3] \\ \tilde{y}'_1[4] \end{bmatrix}, \quad (19)$$

which provides an exact estimate in the absence of noise. We may design the symbols of $x_1[n]$, $x_2[n]$, and $x_r[n]$ that are involved in the coefficient matrix of (19) to guarantee the matrix is invertible.

The ZF initialization provides a starting point close to the optimal solution, which not only reduces the number of iterations for convergence compared to random initialization, but also reduces the likelihood that the algorithm will trap in a local minimum far from the optimal solution.

D. BFGS Algorithm

After we obtain all the required inputs of the algorithm, it is summarized as the following:

Initialize: $\mathbf{x}_{\{p\}}^0 \triangleq [\hat{p}_x^T \hat{p}_y^T]^T$, $\mathbf{x}_{\{q\}}^0 \triangleq [\hat{q}_x^T \hat{q}_y^T]^T$, $\mathbf{x}_{\{d\}}^0 \triangleq [\hat{d}_x \hat{d}_y]^T$,

$$\mathbf{x}_{\{\theta\}}^0 \triangleq [\hat{\theta}_x \hat{\theta}_y]^T, \mathbf{x}_{\{h_{11}\}}^0 \triangleq [\hat{h}_{11x} \hat{h}_{11y}]^T.$$

Repeat until convergence for $i \geq 1$:

Step 1: $\mathbf{x}_0^{(i)} = \mathbf{x}_{\{p\}}^{(i-1)}$, $\mathbf{B}_0^{-1} = \mathbf{I}_2$

Step 2: Repeat until convergence for k : (BFGS)

1. Obtain a search direction $\mathbf{p}_k = -\mathbf{B}_k^{-1} \nabla f(\mathbf{x}_k^{(i)})$.

2. Find stepsize α_k by backtracking linesearch,

then update $\mathbf{x}_{k+1}^{(i)} = \mathbf{x}_k^{(i)} + \alpha_k \mathbf{p}_k$.

3. Set $\mathbf{s}_k = \alpha_k \mathbf{p}_k$, $\mathbf{v}_k = \nabla f(\mathbf{x}_{k+1}^{(i)}) - \nabla f(\mathbf{x}_k^{(i)})$

4. Update the inverse Hessian approximation by

$$\mathbf{B}_{k+1}^{-1} = \mathbf{B}_k^{-1} + \frac{(s_k^T v_k + v_k^T B_k^{-1} v_k) s_k s_k^T}{(s_k^T v_k)^2} - \frac{B_k^{-1} v_k s_k^T + s_k v_k^T B_k^{-1}}{s_k^T v_k}$$

Step 3: Obtain the converged result $\mathbf{x}_{\{p\}}^{(i)} = \mathbf{x}_k^{(i)}$

Step 4: Repeat **Step 1** to **Step 3** for q , d , h_{11} , and θ

with $\mathbf{x}_0^{(i)} = \mathbf{x}_{\{q\}}^{(i-1)}$, $\mathbf{x}_0^{(i)} = \mathbf{x}_{\{d\}}^{(i-1)}$, $\mathbf{x}_0^{(i)} = \mathbf{x}_{\{h_{11}\}}^{(i-1)}$,

and $\mathbf{x}_0^{(i)} = \mathbf{x}_{\{\theta\}}^{(i-1)}$ respectively

There are three inputs of the algorithm: (i) received training data from (8), (ii) gradients of the real part and imaginary part of the parameters which are derived in Appendix A (from (63) to (70)), and (iii) the initialization of the parameters which can be obtained from (17) and (19) in Section III-C. For each parameter in ω , after the initial values are given, it is optimized by BFGS algorithm when the other parameters are fixed. The five parameters are optimized alternatively, which is the iteration controlled by i . The results of the iteration will be used as initial values for the next iteration.

The BFGS algorithm is guaranteed to converge to a local minimum point because it is a descent algorithm. This is the case in our setup as explained next. In Step 2.4, BFGS algorithm updates the inverse Hessian approximation matrix which approximates the true Hessian to reduce complexity. The corresponding equation to update the Hessian approximation matrix is given by

$$\mathbf{A}_{k+1} = \mathbf{A}_k + \frac{\mathbf{v}_k \mathbf{v}_k^T}{\mathbf{v}_k^T \mathbf{s}_k} - \frac{(\mathbf{A}_k \mathbf{s}_k)(\mathbf{A}_k \mathbf{s}_k)^T}{\mathbf{s}_k^T \mathbf{A}_k \mathbf{s}_k}. \quad (20)$$

This is a rank-two update which ensures the Hessian approximation matrix is positive definite [26, Sec 8.3.5]. The positive definite property implies that the search direction $\mathbf{p}_k = -\mathbf{A}_k^{-1} \nabla f(\mathbf{x}_k^{(i)})$ is a descent direction. Thus the algorithm is guaranteed to converge to a minimum. However, for non-convex objective functions, the convergence point may be a local minimum that is not optimal. To avoid this, we use ZF estimates of the parameters to initialize the algorithm as mentioned above.

The complexity consists of the evaluation of three parts: (i) The calculation of gradients, (ii) line search, and (iii) the approximate inverse-Hessian matrix update. For the gradients of (13), the calculation is dominated by the matrix inversion of the covariance matrix \mathbf{C} which has complexity of $O(N^3)$, where N is the length of the training length. For large N , \mathbf{C} asymptotically becomes to a Toeplitz matrix. The complexity of inverting a positive definite Toeplitz matrix is $O(N \log^2 N)$. The line search step requires the calculation of (13) which also includes the matrix inversion. Thus line search has the same complexity as the gradients step. The approximate inverse-Hessian matrix update has the complexity of $O(n^2)$ where n is the number of parameters to be estimated, i.e. the length of ω which is 10. The complexity of this update does not scale with N since $n = 10$ is a constant. Therefore, the total complexity of the BFGS algorithm in one iteration is $O(N \log^2 N)$ for large N . Moreover, based on our observation in the simulation, the algorithm with zero-forcing initialization converges at an average of about 3 iterations, which is 2 less iterations than random initialization. This also reduces the complexity of the algorithm.

IV. BASELINE SCHEMES

In this section we provide two baseline schemes for comparison. One is the multi-block training scheme which works similar to half duplex training. The other is the conventional cross-correlation channel estimation method for ISI channel.

To compare to the proposed one-block training scheme, we propose another training scheme that takes multiple transmission blocks in the training. We discuss how the traditional LS method is applied in the full duplex system. The training phase adopts a relay protocol similar to half duplex which is different from the protocol of the data phase. We still do not assume any feedback channel here. The training consists of four phases. In phase 1, the two sources transmit their training sequences \mathbf{x}_{1t} and \mathbf{x}_{2t} with length N_1 simultaneously. Meanwhile, the two sources receive what they transmit. The relay only receives in this phase. The received signals at source 1 and the relay are \mathbf{y}_{P1} and \mathbf{y}_r . We have

$$\begin{aligned} \mathbf{y}_{P1} &= h_{11} \mathbf{x}_{1t} + \mathbf{v}_{P11}, \\ \mathbf{y}_r &= h_{1r} \mathbf{x}_{1t} + h_{2r} \mathbf{x}_{2t} + \mathbf{v}_{P1r}. \end{aligned} \quad (21)$$

The RSI channel h_{11} can be estimated by source 1 itself. Phase 1 costs one-block time which has N_1 symbols.

In phase 2, the relay scales the received signal from phase 1, then transit this processed signal. The two sources only receive the signal from the relay. The received signal at source 1 is

$$\mathbf{y}_{P2} = \alpha_1 h_{r1} \mathbf{y}_r + \mathbf{n}_{P21} = p_m \mathbf{x}_{1t} + q_m \mathbf{x}_{2t} + d_m \mathbf{v}_{P1r} + \mathbf{v}_{P21}, \quad (22)$$

where $p_m = \alpha_1 h_{r1} h_{1r}$, $q_m = \alpha_1 h_{r1} h_{2r}$, $d_m = \alpha_1 h_{r1}$ and $\alpha_1 = \sqrt{P_r / (2P_s + 1)}$.

Through \mathbf{y}_{P2} , source 1 can estimate two cascaded channels. Phase 2 takes another N_1 symbols. In the first two phases the relay works in half duplex mode. The sources only do full duplex at phase 1. Since the training sequence in phase 2 depends on phase 1, the time cost of phase 2 is also N_1 symbols

From the above two phases, the only unknown channel to source 1 is the RSI channel h_{rr} at the relay. If a feedback channel from the relay to source is possible, in phase 3 the relay could transit and receive its own training signal and estimate h_{rr} , then feedback its estimates to the sources, which is more easier to operate. However, we do not assume feedback channels due to practical reasons. Thus the relay needs to transmit training signal that contains h_{rr} to the sources. Assuming the training sequence sent by the relay is \mathbf{x}_{rt} with length N_2 , the relay transmits it to the sources in phase 3. The received signal is

$$\mathbf{y}_{P3} = h_{r1} \mathbf{x}_{rt} + \mathbf{v}_{P3}. \quad (23)$$

In this phase h_{r1} can be estimated at the source. At the same time, the relay receives its transmitted signal which will be used in the last phase.

In phase 4, the relay transmits its received signal from the last phase, and we have

$$\mathbf{y}_{P4} = h_{r1} \theta \mathbf{x}_{rt} + \alpha_2 h_{r1} \mathbf{v}_{P3r} + \mathbf{v}_{P4}, \quad (24)$$

where $\theta = \alpha_2 h_{rr}$ and $\alpha_2 = \sqrt{P_r / (P_r \sigma_{rr}^2 + 1)}$.

Source 1 is able to estimate the individual channel h_{r1} through \mathbf{y}_{P3} and then recover the other individual channels. The estimate of θ can be obtained by using \mathbf{y}_{P4} . Phase 3 and phase 4 cost another two transmission blocks with block length N_2 . If we assume $N_1 = N_2 = N/4$, then the training

overhead of the multi-block scheme is the same as that of the one-block scheme. Both estimators achieve estimating the individual channels and the RSI channel at each source node.

The estimators are given as follows.

$$\hat{h}_{11} = (\mathbf{x}_{1t}^H \mathbf{x}_{1t})^{-1} \mathbf{x}_{1t}^H \mathbf{y}_{P1}, \quad (25)$$

$$[\hat{p} \ \hat{q}]^T = (\mathbf{X}_{rt}^H \mathbf{X}_{rt})^{-1} \mathbf{X}_{rt}^H \mathbf{y}_{P2}, \quad (26)$$

$$\hat{h}_{r1} = (\mathbf{x}_{rt}^H \mathbf{x}_{rt})^{-1} \mathbf{x}_{rt}^H \mathbf{y}_{P3}, \quad (27)$$

$$\hat{\theta} = (\mathbf{x}_{rt}^H \mathbf{x}_{rt})^{-1} \mathbf{x}_{rt}^H \mathbf{y}_{P4} / \hat{h}_{r1}, \quad (28)$$

where $\mathbf{X}_{rt} = [\mathbf{x}_{1t} \ \mathbf{x}_{2t}]$.

The multi-block scheme is not a bandwidth efficient scheme since it works in half duplex mode. However it has some advantages. First with the switch between the half duplex and full duplex, linear estimator such as LS and MMSE can be applied for channel estimation, in which case we do not need to design special estimators for the system. Second, when the block length in the multi-block scheme is the same as it in one-block scheme, the mean square error (MSE) performance is better than the one-block scheme. Thus, in the multi-block scheme the MSE is improved at the cost of bandwidth.

Another baseline scheme is the correlation method. Using the same signal model in (8), the cross-correlation method for ISI channel can also be applied by treating the taps as different parameters. By using training sequences which has an autocorrelation function that is approximately a delta function, the estimator can be obtained by doing the cross-correlation between the received signal and the training sequences. The parameters $\xi_{\text{ISI}} = [p, q, d, h_{11}, \theta_1, \dots, \theta_{L-1}]^T$, where $\theta_i = \theta^i$ but is treated as different parameters, can be estimated. We directly use the estimate of θ_1 as the final estimates of θ without investigating the the relationship between the channel taps.

V. CRAMER-RAO BOUNDS AND ANALYSIS OF THE FISHER INFORMATION

A. Cramer-Rao Bounds for One-Block Training Scheme

The Cramer-Rao bound is used to evaluate the fundamental limits of each training scheme. We obtain the Fisher information matrix (FIM) through the second order derivative of the likelihood function. We use complex derivatives [27] to find the FIM. We define $\xi = [p \ q \ \theta \ d \ h_{11}]^T$, which has the same parameters as ω , except each entry is a complex variable. The FIM is given by

$$\Gamma(\xi) = \mathbb{E} \left[\frac{\partial f}{\partial \xi^*} \frac{\partial f}{\partial \xi^T} \right]. \quad (29)$$

The (m, n) th element of Γ is given by

$$\Gamma_{mn} = \frac{\partial \boldsymbol{\mu}^H}{\partial \xi_m^*} \mathbf{C}^{-1} \frac{\partial \boldsymbol{\mu}}{\partial \xi_n} + \text{tr} \left(\mathbf{C}^{-1} \frac{\partial \mathbf{C}}{\partial \xi_m^*} \mathbf{C}^{-1} \frac{\partial \mathbf{C}}{\partial \xi_n} \right). \quad (30)$$

We first begin with the diagonal elements of the FIM. For p and q , we have

$$\begin{aligned} \Gamma_{11} &= \frac{\partial \boldsymbol{\mu}^H}{\partial p^*} \mathbf{C}^{-1} \frac{\partial \boldsymbol{\mu}}{\partial p} + \text{tr} \left(\mathbf{C}^{-1} \frac{\partial \mathbf{C}}{\partial p^*} \mathbf{C}^{-1} \frac{\partial \mathbf{C}}{\partial p} \right) \\ &= \mathbf{x}_1^H \mathbf{H}_\theta^H \mathbf{C}^{-1} \mathbf{H}_\theta \mathbf{x}_1, \end{aligned} \quad (31)$$

$$\Gamma_{22} = \mathbf{x}_2^H \mathbf{H}_\theta^H \mathbf{C}^{-1} \mathbf{H}_\theta \mathbf{x}_2. \quad (32)$$

Both $\boldsymbol{\mu}$ and \mathbf{C} contains θ , so

$$\begin{aligned} \Gamma_{33} &= \frac{\partial \boldsymbol{\mu}^H}{\partial \theta^*} \mathbf{C}^{-1} \frac{\partial \boldsymbol{\mu}}{\partial \theta} + \text{tr} \left(\mathbf{C}^{-1} \frac{\partial \mathbf{C}}{\partial \theta^*} \mathbf{C}^{-1} \frac{\partial \mathbf{C}}{\partial \theta} \right) \\ &= (p \mathbf{x}_1 + q \mathbf{x}_2 + d \mathbf{x}_r)^H \mathbf{B}_\theta^H \mathbf{C}^{-1} \mathbf{B}_\theta (p \mathbf{x}_1 + q \mathbf{x}_2 + d \mathbf{x}_r) \\ &\quad + |d|^4 \sigma_n^4 \text{tr} \left(\mathbf{C}^{-1} \mathbf{H}_\theta \mathbf{B}_\theta^H \mathbf{C}^{-1} \mathbf{B}_\theta \mathbf{H}_\theta^H \right), \end{aligned} \quad (33)$$

where $\mathbf{B}_\theta = \frac{\partial \mathbf{H}_\theta}{\partial \theta}$ is also an $N \times N$ Toeplitz matrix given by the first column $[0, 1, 2\theta, \dots, (L-1)\theta^{L-2}, 0, \dots, 0]^T$ and the first row $[0, 0, \dots, 0]$. For d , it is similar to the case of θ since it appears in both $\boldsymbol{\mu}$ and \mathbf{C} ,

$$\begin{aligned} \Gamma_{44} &= \frac{\partial \boldsymbol{\mu}^H}{\partial d^*} \mathbf{C}^{-1} \frac{\partial \boldsymbol{\mu}}{\partial d} + \text{tr} \left(\mathbf{C}^{-1} \frac{\partial \mathbf{C}}{\partial d^*} \mathbf{C}^{-1} \frac{\partial \mathbf{C}}{\partial d} \right) \\ &= \mathbf{x}_r^H \mathbf{H}_\theta^H \mathbf{C}^{-1} \mathbf{H}_\theta \mathbf{x}_r \\ &\quad + |d|^2 \sigma_n^4 \text{tr} \left(\mathbf{C}^{-1} \mathbf{H}_\theta \mathbf{H}_\theta^H \mathbf{C}^{-1} \mathbf{H}_\theta \mathbf{H}_\theta^H \right), \end{aligned} \quad (34)$$

and last for h_{11} ,

$$\begin{aligned} \Gamma_{55} &= \frac{\partial \boldsymbol{\mu}^H}{\partial h_{11}^*} \mathbf{C}^{-1} \frac{\partial \boldsymbol{\mu}}{\partial h_{11}} + \text{tr} \left(\mathbf{C}^{-1} \frac{\partial \mathbf{C}}{\partial h_{11}^*} \mathbf{C}^{-1} \frac{\partial \mathbf{C}}{\partial h_{11}} \right) \\ &= \mathbf{x}_1^H (\mathbf{J}^u)^H \mathbf{J}^u \mathbf{x}_1. \end{aligned} \quad (35)$$

Other elements are given in Appendix B. We focus on these diagonal elements because we will analyze how the channel parameters affect the Fisher information in Section V-B.

The CRBs are given by the diagonal elements of inverse of the FIM such that

$$CRB_{\xi} = \text{tr} \left(\Gamma^{-1} \right). \quad (36)$$

In particular, $CRB_p = [\Gamma^{-1}]_{11}$, $CRB_q = [\Gamma^{-1}]_{22}$, $CRB_\theta = [\Gamma^{-1}]_{33}$, $CRB_d = [\Gamma^{-1}]_{44}$, and $CRB_{h_{11}} = [\Gamma^{-1}]_{55}$ where $[A]_{mn}$ denotes the (m, n) th element of matrix A .

We also derive the CRBs for the multiple transmission blocks training case in Appendix B for comparison with the CRBs of the one-block training scheme.

B. Analysis of the Fisher Information

In this subsection, we analyze the Fisher information for the one-block training scheme by using Szegő's theorem [28], [29] to see how the channel parameters and transmit powers affect the estimation, in the regime where the training length N is large. The asymptotic behavior of Toeplitz matrix \mathbf{H}_θ can thus be analyzed. Define

$$t(\lambda) = \sum_{k=0}^{\infty} t_k e^{j\lambda k}, \quad (37)$$

where $t_k = \theta^k$ for $k = 0, \dots, L-1$ and otherwise $t_k = 0$. Thus, $\mathbf{H}_\theta = \mathbf{T}_N(t(\lambda))$ as $N \rightarrow \infty$. Since \mathbf{H}_θ is a banded Toeplitz matrix, $t(\lambda)$ becomes

$$t(\lambda) = \sum_{k=0}^{L-1} \theta^k e^{j\lambda k} = \frac{1 - \theta^L e^{j\lambda L}}{1 - \theta e^{j\lambda}} = \frac{1}{1 - \theta e^{j\lambda}}, \quad (38)$$

where $\theta^L \approx 0$ by our assumption of channel energy in Section III-A. The covariance matrix \mathbf{C} is

$$\mathbf{C} = |d|^2 \sigma_v^2 \mathbf{T}_N(t(\lambda)) \mathbf{T}_N(t^*(\lambda)) + \sigma_v^2 \mathbf{I}_N. \quad (39)$$

Without loss of generality, we set $\sigma_v^2 = 1$. According to Szegő's theorem, the product of two Toeplitz matrices and the inverse of a Toeplitz matrix are Toeplitz matrices asymptotically. Thus we have

$$\mathbf{C} = |d|^2 \mathbf{T}_N(|t(\lambda)|^2) + \mathbf{I}_N = \mathbf{T}_N(|d|^2 |t(\lambda)|^2 + 1), \quad (40)$$

$$\mathbf{C}^{-1} = \mathbf{T}_N\left(\frac{1}{|d|^2 |t(\lambda)|^2 + 1}\right). \quad (41)$$

Theorem 1: The Fisher information of the cascaded channel p is an increasing function of the absolute value of the RSI channel h_{rr} , a decreasing function of the relay transmit power P_r and the individual channel h_{r1} , and an increasing function of the source transmit power P_s asymptotically when the length of training goes to infinity with fixed training energy.

Proof: The Fisher information of the cascaded channel p in the one-block training scheme from (31) is

$$\Gamma_{11} = \mathbf{x}_1 \mathbf{T}_N(t(\lambda)) \mathbf{T}_N\left(\frac{1}{|d|^2 |t(\lambda)|^2 + 1}\right) \mathbf{T}_N(t^*(\lambda)) \mathbf{x}_1 \quad (42)$$

$$= \mathbf{x}_1 \mathbf{T}_N\left(\frac{|t(\lambda)|^2}{|d|^2 |t(\lambda)|^2 + 1}\right) \mathbf{x}_1 \leq \eta_{\max} \|\mathbf{x}\|^2, \quad (43)$$

where η_{\max} is the maximum eigenvalue of $\mathbf{T}_N\left(\frac{|t(\lambda)|^2}{|d|^2 |t(\lambda)|^2 + 1}\right)$. When $N \rightarrow \infty$, we have

$$\begin{aligned} \eta_{\max} &= \max_{\lambda} \frac{|t(\lambda)|^2}{|d|^2 |t(\lambda)|^2 + 1} = \max_{\lambda} \frac{1}{|d|^2 + |1 - \theta e^{j\lambda}|^2} \\ &= \frac{1}{|d|^2 + |1 - |\theta||^2}, \end{aligned} \quad (44)$$

with λ equals to the minus phase of θ . Therefore, the Fisher information can be expressed in terms of the channel parameters and power scaling factor α ,

$$\Gamma_{11} = \frac{E_t}{\alpha^2 |h_{r1}|^2 + |1 - \alpha |h_{\text{rr}}||^2}, \quad (45)$$

where $E_t = \|\mathbf{x}_1\|^2$ is the training energy and is kept to be a constant.

From the derivation of α to keep the stability of the system in Section III-A, we conclude that $E[|\theta|^2] = \alpha^2 E[|h_{\text{rr}}|^2] < 1$. Proper α can be chosen by using fixed gain margin to satisfy this condition. Thus $|\theta| < 1$ and $|h_{\text{rr}}|$ has a constraint related to α . Therefore, for a constant α , Γ_{11} is an increasing function of $|h_{\text{rr}}|$. It is also a decreasing function of α . Since α grows

with P_r and decreases with P_s , Γ_{11} is a decreasing function of P_r , and an increasing function of P_s . \square

Theorem 1 shows large value of the RSI channel gain increases the Fisher information of the cascaded channel and makes it easier to estimate. On the other hand, Γ_{11} is a decreasing function of α , we can say that increasing P_r does not help to estimate the cascaded channel but increasing P_s does.

Theorem 2: The Fisher information of the RSI channel h_{rr} is an increasing function of $|h_{\text{rr}}|$, the absolute values of both the cascaded channels, and the power scaling factor α asymptotically when the length of training goes to infinity with fixed training energy.

Proof: Define $\mathbf{B}_\theta = \mathbf{T}_N(g(\lambda))$ where $g(\lambda) = \frac{e^{j\lambda}}{(1 - \theta e^{j\lambda})^2}$. Function $g(\lambda)$ is obtained similarly to $t(\lambda)$ by using the sum of a geometric sequence and $\theta^L \approx 0$. Then, from (33), the Fisher information of the RSI channel can be represented by Toeplitz matrices as (46) and upper bounded by (47), shown at the bottom of the page.

For the first term in (47), the maximum value is $\frac{1}{|1 - |\theta||^2 (|d|^2 + |1 - |\theta||^2)}$. The second term comes from the asymptotic property of Toeplitz matrix that the trace of it is equal to the integration of the function that characterized it. Simplifying the integral we have

$$\begin{aligned} &\int_0^{2\pi} \frac{|g(\lambda)|^2 |t(\lambda)|^2}{(|d|^2 |t(\lambda)|^2 + 1)^2} d\lambda \\ &= \int_0^{2\pi} \frac{1}{|1 - \theta e^{j\lambda}|^2 (|d|^2 + |1 - \theta e^{j\lambda}|^2)^2} d\lambda. \end{aligned} \quad (48)$$

In the full duplex two-way relay system, we assume $P_r \gg P_s$ since P_s is the received power at the relay which incorporates the pathloss. Thus $\alpha^2 \gg 1$. Note that $|\theta| < 1$, we have $|d|^2 = \alpha^2 |h_{r1}|^2 \gg |1 - \theta e^{j\lambda}|^2$. We can approximately calculate the integral as

$$\begin{aligned} &\frac{1}{2\pi} \int_0^{2\pi} \frac{1}{|1 - \theta e^{j\lambda}|^2 (|d|^2 + |1 - \theta e^{j\lambda}|^2)^2} d\lambda \\ &\approx \frac{1}{2\pi} \int_0^{2\pi} \frac{1}{|1 - \theta e^{j\lambda}|^2 |d|^4} d\lambda = \frac{1}{|d|^4} \frac{1}{(|\theta| + 1)|\theta| - 1}. \end{aligned} \quad (49)$$

The Fisher information of the RSI channel θ becomes

$$\begin{aligned} \Gamma_{33} &= \frac{\alpha^2 E_t (|h_{r1} h_{1r}|^2 + |h_{r1} h_{2r}|^2 + |h_{r1}|^2)}{|1 - \alpha |h_{\text{rr}}||^2 (\alpha^2 |h_{r1}|^2 + |1 - \alpha |h_{\text{rr}}||^2)} \\ &+ \frac{E_t}{P_s (\alpha |h_{\text{rr}}| + 1) |\alpha |h_{\text{rr}}| - 1}. \end{aligned} \quad (51)$$

Γ_{33} is an increasing function of α so that increasing P_r helps to estimate h_{rr} while increasing P_s does not. Γ_{33} is

$$\Gamma_{33} = (p\mathbf{x}_1 + q\mathbf{x}_2 + d\mathbf{x}_r)^H \mathbf{T}_N\left(\frac{|g(\lambda)|^2}{|d|^2 |t(\lambda)|^2 + 1}\right) (p\mathbf{x}_1 + q\mathbf{x}_2 + d\mathbf{x}_r) + |d|^4 \text{tr}\left(\mathbf{T}_N\left(\frac{|g(\lambda)|^2 |t(\lambda)|^2}{(|d|^2 |t(\lambda)|^2 + 1)^2}\right)\right) \quad (46)$$

$$\leq (|p|^2 \|\mathbf{x}_1\|^2 + |q|^2 \|\mathbf{x}_2\|^2 + |d|^2 \|\mathbf{x}_r\|^2) \max_{\lambda} \left(\frac{|g(\lambda)|^2}{|d|^2 |t(\lambda)|^2 + 1}\right) + |d|^4 \frac{E_t}{2\pi P_s} \int_0^{2\pi} \frac{|g(\lambda)|^2 |t(\lambda)|^2}{(|d|^2 |t(\lambda)|^2 + 1)^2} d\lambda. \quad (47)$$

$$\Gamma_{\text{diff}} = \Gamma_{33} - \Gamma_{\theta_1} = \underbrace{(p\mathbf{H}_\theta \mathbf{x}_1 + q\mathbf{H}_\theta \mathbf{x}_2 + d\mathbf{x}_r)^H \mathbf{T}_N \left(\frac{|g(\lambda)|^2 - 1}{|d|^2 |t(\lambda)|^2 + 1} \right) (p\mathbf{H}_\theta \mathbf{x}_1 + q\mathbf{H}_\theta \mathbf{x}_2 + d\mathbf{x}_r)}_{\Gamma_a} + \underbrace{|d|^4 \text{tr} \left(\mathbf{T}_N \left(\frac{|t(\lambda)|^2 (|g(\lambda)|^2 - 1)}{(|d|^2 |t(\lambda)|^2 + 1)^2} \right) \right)}_{\Gamma_b}. \quad (54)$$

$$\Gamma_a \leq \left(|p|^2 \|\mathbf{x}_1\|^2 + |q|^2 \|\mathbf{x}_2\|^2 + |d|^2 \|\mathbf{x}_r\|^2 \right) \max_{\lambda} \left(\frac{|g(\lambda)|^2 - 1}{|d|^2 |t(\lambda)|^2 + 1} \right) \\ = \left(|p|^2 \|\mathbf{x}_1\|^2 + |q|^2 \|\mathbf{x}_2\|^2 + |d|^2 \|\mathbf{x}_r\|^2 \right) \frac{1 - (1 - |\theta|)^4}{|d|^2 (1 - |\theta|^2) + (1 - |\theta|^4)}. \quad (55)$$

also a function of $|h_{r1}|$ and it increases with growing $|h_{r1}|$. That means larger RSI channel will make itself easier to estimate. Lastly, Γ_{33} is an increasing function of channel gains between sources and relay, thus large channel gains increase the accuracy of the estimate of h_{r1} .

Theorem 3: The Fisher information of the individual channel h_{r1} is an increasing function of the absolute value of the RSI channel h_{r1} , a decreasing function of the power scaling factor α , and a decreasing function of the absolute value of h_{r1} asymptotically when the length of training goes to infinity with fixed training energy.

Proof: Similar to the above two proofs, for the relay to source channel h_{r1} , we have

$$\Gamma_{44} = \frac{E_t}{\alpha^2 |h_{r1}|^2 + |1 - \alpha |h_{r1}||^2} + \frac{E_t}{P_s (\alpha |h_{r1}| + 1) |\alpha |h_{r1}| - 1|}. \quad (52)$$

The first term of (52) is the same as (45). The second term is similar to the second term in (51) and can be obtained by using (48) to (50). \square

The affects of RSI channel and α to estimating h_{r1} are the same to the cascaded channel case. However the Fisher information of h_{r1} contains itself so that it will be harder to estimate the channel when it has large absolute value.

C. Exploiting the Structure of the Related Channel Taps

To show the advantage of exploiting the channel structure created by the RSI feedback, we compare the Fisher information of the RSI channel θ corresponding to two channel assumptions in one-block training scheme. In the first case, the structure of geometric sequence ISI channel taps is considered, while in the other case the channel taps are treated as different parameters (not necessarily a geometric sequence). We will show that exploiting the channel structure has larger Fisher information than treating the taps as different parameters.

We first look at the Fisher information of treating the taps as different parameters. The parameter vector for this case is defined by $\boldsymbol{\xi}_{\text{ISI}} = [p, q, d, h_{11}, \theta_1, \dots, \theta_{L-1}]^T$, where θ_i are independent channel taps. The Fisher information of p, q, d , and h_{11} are the same as the Fisher information of exploiting the channel structure. Let the partial derivative of \mathbf{H}_θ with respect to θ_1 be $\mathbf{D}_1 = \frac{\partial \mathbf{H}_\theta}{\partial \theta_1} = \mathbf{J}^d$. \mathbf{D}_1 is also a Toeplitz matrix

and thus we have $\mathbf{D}_1 = \mathbf{T}_N(e^{j\lambda})$. The Fisher information for θ_1 is similar to (33) which is

$$\Gamma_{\theta_1} = (p\mathbf{x}_1 + q\mathbf{x}_2 + d\mathbf{x}_r)^H \mathbf{D}_1^H \mathbf{C}^{-1} \mathbf{D}_1 (p\mathbf{x}_1 + q\mathbf{x}_2 + d\mathbf{x}_r) + |d|^4 \sigma_n^4 \text{tr} \left(\mathbf{C}^{-1} \mathbf{H}_\theta \mathbf{D}_1^H \mathbf{C}^{-1} \mathbf{D}_1 \mathbf{H}_\theta^H \right). \quad (53)$$

Theorem 4: With designed training sequences, the Fisher information of θ is greater than that of θ_1 by Γ_{diff} which can be approximated in closed form, when training length goes to infinity.

Proof: The difference of the two Fisher information is Γ_{diff} in (54), shown at the top of the page.

For the first term of (54), we have the inequality in (55), shown at the top of the page. The equality holds when the training sequence is the eigenvector corresponding to the maximum eigenvalue of $\mathbf{T}_N \left(\frac{|g(\lambda)|^2 - 1}{|d|^2 |t(\lambda)|^2 + 1} \right)$ which is given by $\frac{1}{\sqrt{N}} [1, e^{j2\pi}, e^{j4\pi}, \dots, e^{j2\pi(N-1)}]^T$. Note that $|\theta| < 1$, therefore, by choosing the training sequence, the first term of the difference is greater than zero.

For the second term, first we calculate

$$\frac{1}{2\pi} \int_0^{2\pi} |g(\lambda)|^2 d\lambda = \left(\frac{1 + |\theta|^2}{(1 - |\theta|^2)^3} \cdot \text{sign}(1 - |\theta|^2) \right). \quad (56)$$

Then, the integration in Γ_b can be approximated by using integration by parts and the results from (48) to (50) and (56), we have

$$\Gamma_b = \frac{1 - |1 - \theta|^4}{|1 - \theta|^4 (|\theta| + 1) |\theta| - 1|} - \frac{1}{2\pi} \int_0^{2\pi} \frac{(|g(\lambda)|^2)'}{|1 - \theta e^{j\lambda}|^2} d\lambda \\ = \frac{1 - |1 - \theta|^4}{|1 - \theta|^4 (|\theta| + 1) |\theta| - 1|} - \frac{1}{2\pi} \int_0^{2\pi} \frac{-4|\theta| \sin \lambda}{|1 - \theta e^{j\lambda}|^8} \\ (57)$$

$$= \frac{1 - |1 - \theta|^4}{|1 - \theta|^4 (|\theta| + 1) |\theta| - 1|}, \quad (58)$$

where the second term in (57) is zero since it is an odd function over $[0, 2\pi]$. $\Gamma_b > 0$ for $|\theta| < 1$. Thus, $\Gamma_{\text{diff}} = \Gamma_a + \Gamma_b > 0$. \square

The Fisher information of related channel taps is larger than independent channel taps, regardless of estimators so that exploiting the structure arising from the RSI channel increases its Fisher information.

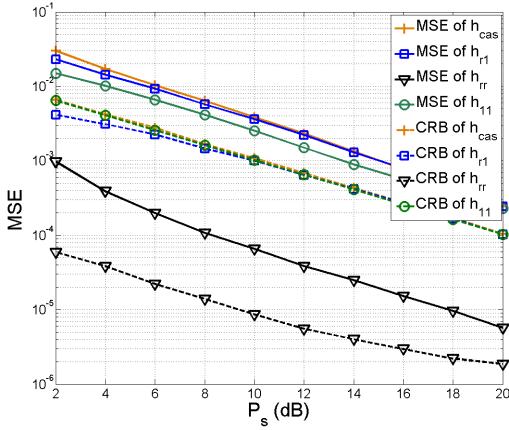


Fig. 2. MSE of the one block training scheme.

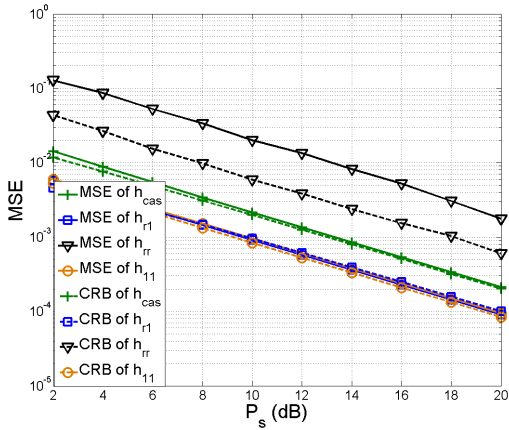


Fig. 3. MSE of the multiple-block training scheme.

VI. NUMERICAL RESULTS

In our simulations, we first setup a set of parameters and keep it unchanged for all the training schemes. We set the relay power $P_r = 40$ dB and the RSI variance $\sigma_{\text{rr}}^2 = -20$ dB. If the original self-interference channel has unit variance, then the RSI variance σ_{rr}^2 represents the ability of self-interference cancellation to reduce the interference power. We first simulate the MSEs of estimates of the channels to show the performance of the ML estimator in the one-block training scheme with training length $N = 100$. Figure 2 shows the MSEs of different channel parameters. For the cascaded channel, we plot the MSE of $h_{\text{cas}} = h_{\text{r1}}h_{\text{r}} = p/\alpha$ which is the channel without power scaling factors for comparison with other schemes. The other cascaded channel q/α is omitted since it has a symmetric position to p/α and similar results. In Figure 2 and 3, h_{r1} represents the individual channel from the relay to source 1, and h_{rr} and h_{11} are the RSI channels in the relay and source 1 respectively. The MSEs are compared with the CRBs obtained by (31) to (35). It can be observed that there is a gap between MSE and CRB because the block length which is also the overhead in the one-block scheme N is not large enough. Since the ML estimator is asymptotic efficient, i.e. achieves the CRB as N goes to infinity [27], we expect this gap to close for large N .

The MSEs and CRBs for the two baseline methods are also simulated. Figure 3 shows the performance of the LS

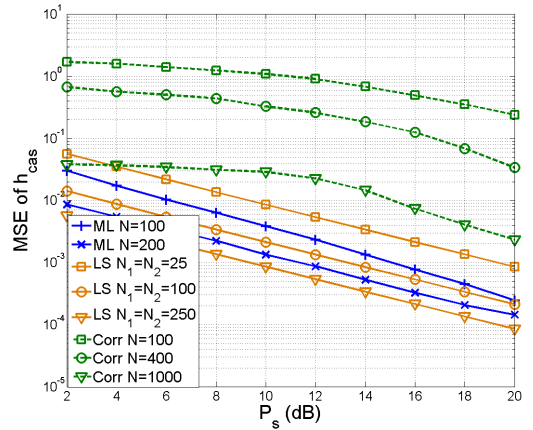
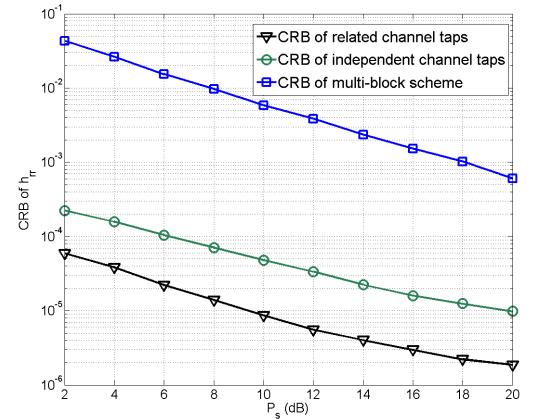


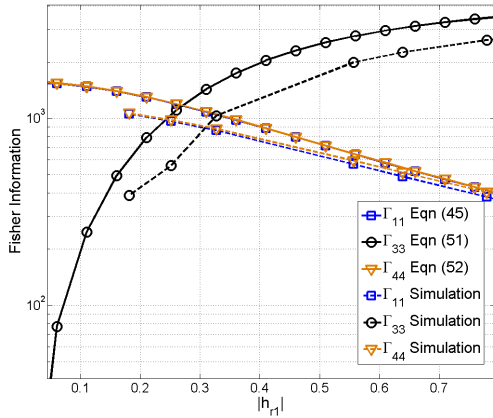
Fig. 4. MSE performance comparison of different training schemes.

Fig. 5. Comparison of CRBs of h_{rr} with and without exploiting the structure of related channel taps.

estimator in the multi-block training scheme. Here we set $N_1 = N_2 = 100$ which means this scheme has the same training block length as the one block training scheme. To keep a fair comparison, the training power of the relay in the multi-block training is $P_r = P_s$, same as the one-block training scheme.

In Figure 4, the MSE performance of the cascaded channel h_{cas} for different training schemes are compared. If the overhead of training is kept the same, which means the $N_1 = N_2 = N/4$, the one-block training scheme has better performance than the multi-block training, and the cross-correlation method. However, the multi-block training scheme outperforms the one-block training scheme when the training block lengths, which is fixed, of both schemes are the same. This is expected since the LS estimator keeps the same transmit power as the ML estimator for both nodes but takes four times the transmit time for training. When the overhead increases, all the schemes have lower MSEs.

The CRBs of the RSI channel h_{rr} for different schemes are shown in Figure 5. The MSE of h_{rr} for the cross-correlation method is also shown in this figure. The cross-correlation method has large gap between the MSE and CRB because the autocorrelation function of the training sequence is not a perfect delta function with limited training length. The CRBs with and without exploiting the structure of related channel

Fig. 6. Fisher information vs $|h_{r1}|$.

taps are also compared. Exploiting the structure has lower CRB than treating the taps as different parameters in one-block training scheme. We also see that the CRB of the multi-block training scheme is higher than those of one-block training scheme when overhead is fixed.

In Figure 6, we compare the Fisher information calculated by (45), (51), and (52) and that from simulation results. The Fisher information Γ_{11} , Γ_{33} , Γ_{44} are for the cascaded channel h_{cas} , RSI channel h_{rr} , and the individual channel h_{r1} in the one-block training scheme respectively. The figure shows Γ_{11} and Γ_{44} decreases while Γ_{33} increases with increasing $|h_{r1}|$, which verifies Theorem 1 to 3. We can conclude from Figure 6 that large gain of the individual channel helps to estimate the individual channel and it does not help to estimate the cascaded channel and the RSI channel. We set training length as $N = 100$ in this simulation. There is a gap between the simulated Fisher information and the analytical one since the analytical Fisher information expression is obtained in the asymptotic regime when N is large. For Γ_{11} and Γ_{44} the gaps are negligible and for Γ_{33} the gap is within a factor of 1.3.

The difference in Fisher information with the channel structure versus treating the taps as individual variables, which is Γ_{diff} , is also simulated and compared to that calculated from (55) and (58) in Figure 7. When using $N = 100$ in the simulation, the gap between the theory and simulation for the difference in Fisher information is around a factor of 1.6, illustrating the usefulness of (55) and (58). From the simulation we observe that the analysis of the asymptotic behavior of the Fisher information is close to the simulation results. Figure 7 verifies Theorem 4 which asserts that taking the channel structure into account is always better than treating the taps as individual variables when estimating the RSI channel. Figure 7 also shows increasing P_r helps to estimate the RSI channel which is concluded in Theorem 3.

To illustrate the benefit of canceling RSI at the receiver by using the estimates of θ , BER performance with different detectors are simulated. We implemented two detectors: (i) an equalizer using Viterbi algorithm which uses the full information of channel taps, (ii) a matched filter with the strongest channel tap. In this simulation, estimated CSI are used. We also simulate the effect of noise whitening. Figure 8 shows the comparison of BER of the two detectors with a fixed

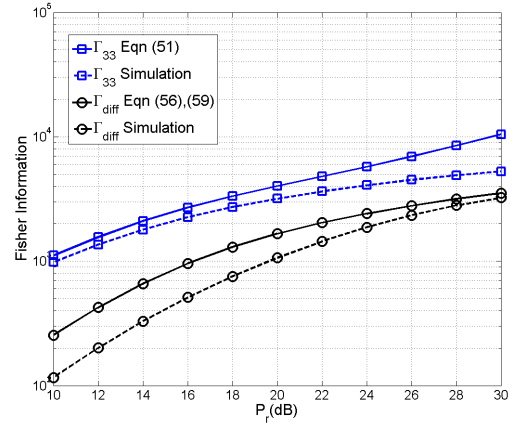
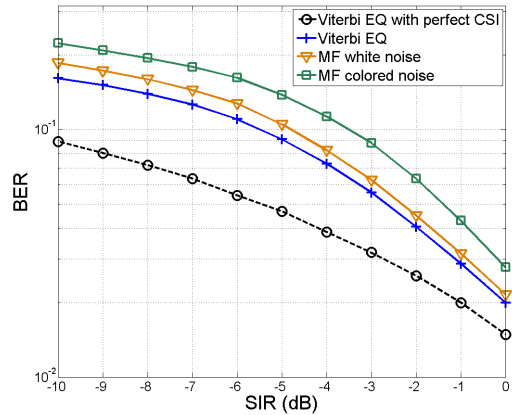
Fig. 7. Fisher information vs relay transmit power P_r .

Fig. 8. BER performance for different detectors.

relay power $P_r = 40$ dB. Define the signal to interference ratio at relay as

$$\text{SIR}_r = \frac{\text{E}[|h_{1r}x_{1d}[n] + h_{2r}x_{2d}[n]|^2]}{t_{rd}[n]} = \frac{2P_s}{P_r\sigma_{rr}^2}. \quad (59)$$

Note that σ_{rr}^2 is the variance of the RSI after the self-interference cancellation at the relay. Since P_s actually represents the power of the source transmitted signal arriving at the relay, according to the data reported in [3] and [11], it could be much smaller than the self-interference power from the relay itself, even after some method of cancellation. This case become more severe when the full duplex transceiver is a base station. Thus SIR_r can be negative in dB scale. Figure 8 shows the BER performance for different detectors. For the whitened noise case, the Viterbi equalizer outperforms the matched filter detector by about 1.5 dB in this important low SIR regime showing that the ISI due to the RSI cannot be ignored. This advantage decreases with increasing SIR since the RSI becomes lower. There is also a gap of about 1dB between the two matched filter detectors with and without noise whitening. Thus, whitening the noise not only limits the maximum signal power but also improves the BER. It shows one advantage of estimating the individual channel rather than only estimating the cascaded channel. However, when SIR_r increases, the gap between the equalizer and matched filter decreases since RSI becomes rather small and the ISI effect can be ignored.

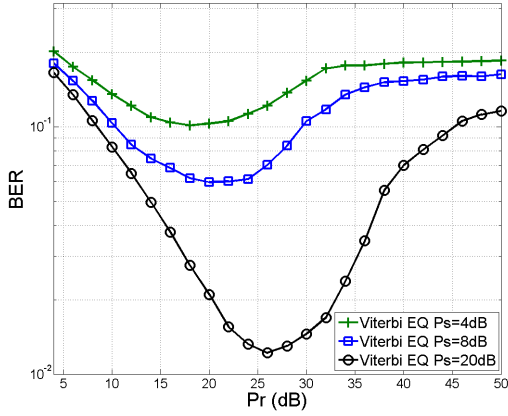


Fig. 9. BER performance for different combinations of P_r and P_s .

Figure 9 shows the BER performance varying with P_r . For a fixed P_s , the BER first reduces and then goes up with increasing P_r . The destination source will have high SNR when the relay transmits with large P_r so increasing it helps to improve the BER performance. However, continuing to increase P_r results in worse BER because the RSI power is also related to P_r and the desired signal is overwhelmed by interference when P_r is too large. On the other hand, for a fixed P_r , increasing P_s always reduces the BER because the SIR_r is proportional to P_s . In summary, increasing P_s always helps to improve the BER but increasing P_r does not; BER first decreases and then increases since the RSI also increases with P_r .

VII. CONCLUSION

The one-block training schemes and two baselines for full duplex two-way relays are proposed in this paper to obtain the CSI in the presence of RSI. With one-block training scheme, an ML estimator is derived to estimate the cascaded channel, individual channel as well as the RSI channel simultaneously. The BFGS algorithm is used in the calculation of the ML estimator. The initialization and convergence of the algorithm are also discussed. The two baselines, the multi-block training scheme with LS estimator and the cross-correlation method, are proposed for comparison. The CRBs for the three schemes are derived. By using the asymptotic properties of Toeplitz matrices, how the channel parameters and transmit powers affect the Fisher information is analyzed. We also showed analytically that the Fisher information of exploiting the structure of the channel taps is greater than that of treating the taps as individual variables.

APPENDIX A

GRADIENTS USED IN THE BFGS METHOD

We derive the gradients used in the BFGS method in this appendix. Before that the following derivatives are needed.

$$\frac{\partial \boldsymbol{\mu}}{\partial \theta_x} = \mathbf{B}_\theta (\mathbf{X}_t \mathbf{h} + d \mathbf{x}_r), \quad \frac{\partial \boldsymbol{\mu}}{\partial \theta_y} = j \mathbf{B}_\theta (\mathbf{X}_t \mathbf{h} + d \mathbf{x}_r), \quad (60)$$

$$\frac{\partial \mathbf{C}}{\partial \theta_x} = |d|^2 \sigma_n^2 (\mathbf{B}_\theta \mathbf{H}_\theta^H + \mathbf{H}_\theta \mathbf{B}_\theta^H), \quad (61)$$

$$\frac{\partial \mathbf{C}}{\partial \theta_y} = |d|^2 \sigma_n^2 (j \mathbf{B}_\theta \mathbf{H}_\theta^H - j \mathbf{H}_\theta \mathbf{B}_\theta^H), \quad (62)$$

where $\mathbf{B}_\theta = \frac{\partial \mathbf{H}_\theta}{\partial \theta}$ is also an $N \times N$ Toeplitz matrix given by the first column $[0, 1, 2\theta, \dots, (L-1)\theta^{L-2}, 0, \dots, 0]^T$ and the first row $[0, 0, \dots, 0]$.

The gradients for both real and imaginary part are needed as inputs of the algorithm. The gradients of p_x and p_y are

$$\nabla f_{p_x} = \frac{\partial f}{\partial p_x} = -2\text{Re} \left[(\mathbf{y}_1 - \boldsymbol{\mu})^H \mathbf{C}^{-1} \mathbf{H}_\theta \mathbf{x}_1 \right], \quad (63)$$

$$\nabla f_{p_y} = \frac{\partial f}{\partial p_y} = -2\text{Re} \left[(\mathbf{y}_1 - \boldsymbol{\mu})^H \mathbf{C}^{-1} j \mathbf{H}_\theta \mathbf{x}_1 \right]. \quad (64)$$

The derivatives of q are similar to those of p only by replacing \mathbf{x}_1 with \mathbf{x}_2 in (63). The derivatives with respect to h_{11} are

$$\nabla f_{h_{11x}} = \frac{\partial f}{\partial h_{11x}} = -2\text{Re} \left[(\mathbf{y}_1 - \boldsymbol{\mu})^H \mathbf{C}^{-1} \mathbf{J}^u \mathbf{x}_1 \right], \quad (65)$$

$$\nabla f_{h_{11y}} = \frac{\partial f}{\partial h_{11y}} = -2\text{Re} \left[(\mathbf{y}_1 - \boldsymbol{\mu})^H \mathbf{C}^{-1} j \mathbf{J}^u \mathbf{x}_1 \right]. \quad (66)$$

For d , it's involved in both $\boldsymbol{\mu}$ and \mathbf{C} , thus

$$\nabla f_{d_x} = \text{tr} \left(2d_x \mathbf{C}^{-1} \mathbf{H}_\theta \mathbf{H}_\theta^H \right) - 2\text{Re} \left[(\mathbf{y}_1 - \boldsymbol{\mu})^H \mathbf{C}^{-1} \mathbf{H}_\theta \mathbf{x}_r \right] - (\mathbf{y}_1 - \boldsymbol{\mu})^H \mathbf{C}^{-1} (2d_x \mathbf{H}_\theta \mathbf{H}_\theta^H) \mathbf{C}^{-1} (\mathbf{y}_1 - \boldsymbol{\mu}), \quad (67)$$

$$\nabla f_{d_y} = \text{tr} \left(2d_y \mathbf{C}^{-1} \mathbf{H}_\theta \mathbf{H}_\theta^H \right) - 2\text{Re} \left[(\mathbf{y}_1 - \boldsymbol{\mu})^H \mathbf{C}^{-1} j \mathbf{H}_\theta \mathbf{x}_r \right] - (\mathbf{y}_1 - \boldsymbol{\mu})^H \mathbf{C}^{-1} (2d_y \mathbf{H}_\theta \mathbf{H}_\theta^H) \mathbf{C}^{-1} (\mathbf{y}_1 - \boldsymbol{\mu}), \quad (68)$$

and θ is similar to d for which we need the derivatives of $\boldsymbol{\mu}$ and \mathbf{C} with respect with it. Using (60) and (62), we have

$$\begin{aligned} \nabla f_{\theta_x} &= \text{tr} \left(|d|^2 \sigma_n^2 \mathbf{C}^{-1} (\mathbf{B}_\theta \mathbf{H}_\theta^H + \mathbf{H}_\theta \mathbf{B}_\theta^H) \right) \\ &\quad - 2\text{Re} \left[(\mathbf{y}_1 - \boldsymbol{\mu})^H \mathbf{C}^{-1} \mathbf{B}_\theta (p \mathbf{x}_1 + q \mathbf{x}_2 + d \mathbf{x}_r) \right] \\ &\quad - |d|^2 \sigma_n^2 (\mathbf{y}_1 - \boldsymbol{\mu})^H \mathbf{C}^{-1} (\mathbf{B}_\theta \mathbf{H}_\theta^H + \mathbf{H}_\theta \mathbf{B}_\theta^H) \\ &\quad \times \mathbf{C}^{-1} (\mathbf{y}_1 - \boldsymbol{\mu}), \end{aligned} \quad (69)$$

$$\begin{aligned} \nabla f_{\theta_y} &= \text{tr} \left(|d|^2 \sigma_n^2 \mathbf{C}^{-1} (j \mathbf{B}_\theta \mathbf{H}_\theta^H - j \mathbf{H}_\theta \mathbf{B}_\theta^H) \right) \\ &\quad - 2\text{Re} \left[(\mathbf{y}_1 - \boldsymbol{\mu})^H \mathbf{C}^{-1} \mathbf{B}_\theta j (p \mathbf{x}_1 + q \mathbf{x}_2 + d \mathbf{x}_r) \right] \\ &\quad - |d|^2 \sigma_n^2 (\mathbf{y}_1 - \boldsymbol{\mu})^H \mathbf{C}^{-1} (j \mathbf{B}_\theta \mathbf{H}_\theta^H - j \mathbf{H}_\theta \mathbf{B}_\theta^H) \\ &\quad \times \mathbf{C}^{-1} (\mathbf{y}_1 - \boldsymbol{\mu}). \end{aligned} \quad (70)$$

APPENDIX B

ELEMENTS OF FISHER INFORMATION MATRIX

For the one-block training scheme, elements for the FIM can be obtained by (30). We derive all the Γ_{mn} , $m \neq n$ here. For different (m, n) , they are given by the following.

$$\begin{aligned} \Gamma_{12} &= \mathbf{x}_1^H \mathbf{H}_\theta^H \mathbf{C}^{-1} \mathbf{H}_\theta \mathbf{x}_2, \\ \Gamma_{13} &= \mathbf{x}_1^H \mathbf{H}_\theta^H \mathbf{C}^{-1} \mathbf{B}_\theta (p \mathbf{x}_1 + q \mathbf{x}_2 + d \mathbf{x}_r), \\ \Gamma_{14} &= \mathbf{x}_1^H \mathbf{H}_\theta^H \mathbf{C}^{-1} \mathbf{H}_\theta \mathbf{x}_r, \quad \Gamma_{15} = \mathbf{x}_1^H \mathbf{H}_\theta^H \mathbf{C}^{-1} \mathbf{J}^u \mathbf{x}_1, \\ \Gamma_{23} &= \mathbf{x}_2^H \mathbf{H}_\theta^H \mathbf{C}^{-1} \mathbf{B}_\theta (p \mathbf{x}_1 + q \mathbf{x}_2 + d \mathbf{x}_r), \\ \Gamma_{24} &= \mathbf{x}_2^H \mathbf{H}_\theta^H \mathbf{C}^{-1} \mathbf{H}_\theta \mathbf{x}_r, \quad \Gamma_{25} = \mathbf{x}_2^H \mathbf{H}_\theta^H \mathbf{C}^{-1} \mathbf{J}^u \mathbf{x}_1, \\ \Gamma_{35} &= (p \mathbf{x}_1 + q \mathbf{x}_2 + d \mathbf{x}_r)^H \mathbf{B}_\theta^H \mathbf{C}^{-1} \mathbf{J}^u \mathbf{x}_1, \\ \Gamma_{45} &= \mathbf{x}_r^H \mathbf{H}_\theta^H \mathbf{C}^{-1} \mathbf{J}^u \mathbf{x}_1, \\ \Gamma_{34} &= (p \mathbf{x}_1 + q \mathbf{x}_2 + d \mathbf{x}_r)^H \mathbf{B}_\theta^H \mathbf{C}^{-1} \mathbf{H}_\theta \mathbf{x}_r \\ &\quad + d^* |d|^2 \sigma_n^4 \text{tr} \left(\mathbf{C}^{-1} \mathbf{H}_\theta \mathbf{B}_\theta^H \mathbf{C}^{-1} \mathbf{H}_\theta \mathbf{H}_\theta^H \right), \end{aligned} \quad (71)$$

and $\Gamma_{mn} = \Gamma_{nm}^*$.

We also derive the CRBs for the multi-block training scheme. Put (21) to (24) together to form a new received signal vector as

$$\mathbf{y}_M = \begin{bmatrix} \mathbf{y}_{P2}^T & \mathbf{y}_{P4}^T & \mathbf{y}_{P3}^T & \mathbf{y}_{P1}^T \end{bmatrix}^T, \quad (72)$$

The mean of \mathbf{y}_M is given by

$$\boldsymbol{\mu}_M = \begin{bmatrix} \boldsymbol{\mu}_h^T & \boldsymbol{\mu}_\theta^T & \boldsymbol{\mu}_{h_{r1}}^T & \boldsymbol{\mu}_{h_{11}}^T \end{bmatrix}^T, \quad (73)$$

where $\boldsymbol{\mu}_h = p\mathbf{x}_{1t} + q\mathbf{x}_{2t}$, $\boldsymbol{\mu}_\theta = h_{r1}\theta\mathbf{x}_{rt}$, $\boldsymbol{\mu}_{h_{r1}} = h_{r1}\mathbf{x}_{rt}$, and $\boldsymbol{\mu}_{h_{11}} = h_{11}\mathbf{x}_{1t}$.

The covariance matrix of \mathbf{y}_M is

$$\begin{aligned} \mathbf{C}_M &= \begin{bmatrix} \mathbf{C}_h & 0 & 0 & 0 \\ 0 & \mathbf{C}_\theta & 0 & 0 \\ 0 & 0 & \mathbf{C}_{h_{r1}} & 0 \\ 0 & 0 & 0 & \mathbf{C}_{h_{11}} \end{bmatrix} \\ &= \sigma_v^2 \begin{bmatrix} \alpha_1^2|h_{r1}|^2 + 1 & 0 & 0 & 0 \\ 0 & \alpha_2^2|h_{r1}|^2 + 1 & 0 & 0 \\ 0 & 0 & 1 & 0 \\ 0 & 0 & 0 & 1 \end{bmatrix} \otimes \mathbf{I}_N, \end{aligned} \quad (74)$$

where \otimes denotes the Kronecker product. $\boldsymbol{\mu}_M$ is a $4N \times 1$ vector and \mathbf{C}_M is a $4N \times 4N$ diagonal matrix due to the uncorrelated noise in \mathbf{y}_M .

Define $\boldsymbol{\xi}^{(M)} = [p \ q \ \theta \ h_{r1} \ h_{11}]^T$. The likelihood function is

$$p(\mathbf{y}_M; \boldsymbol{\xi}^{(M)}) = \frac{1}{\pi^N |\mathbf{C}|} \exp\left(-(\mathbf{y}_M - \boldsymbol{\mu}_M)^H \mathbf{C}_M^{-1} (\mathbf{y}_M - \boldsymbol{\mu}_M)\right). \quad (75)$$

The (m, n) th element of the FIM is given by

$$\Gamma_{mn}^{(M)} = \frac{\partial \boldsymbol{\mu}_M^H}{\partial (\xi_m^{(M)})^*} \mathbf{C}_M^{-1} \frac{\partial \boldsymbol{\mu}_M}{\partial \xi_n^{(M)}} + \text{tr} \left(\mathbf{C}_M^{-1} \frac{\partial \mathbf{C}_M}{\partial (\xi_m^{(M)})^*} \mathbf{C}_M^{-1} \frac{\partial \mathbf{C}_M}{\partial \xi_n^{(M)}} \right). \quad (76)$$

Only the diagonal elements, $\Gamma_{12}^{(M)}$, and $\Gamma_{21}^{(M)}$ are not zero. Thus the inverse of the FIM can be obtained by finding the inverse of a partitioned matrix. Define $\mathbf{D} = \Gamma_{11}^{(M)} \Gamma_{22}^{(M)} - \Gamma_{12}^{(M)} \Gamma_{21}^{(M)}$. The CRBs are given by the diagonal elements of inverse of the FIM, thus

$$\begin{aligned} CRB_p^{(M)} &= \left[(\boldsymbol{\Gamma}^{(M)})^{-1} \right]_{11} = \Gamma_{22}^{(M)} / \mathbf{D}, \\ CRB_q^{(M)} &= \left[(\boldsymbol{\Gamma}^{(M)})^{-1} \right]_{22} = \Gamma_{11}^{(M)} / \mathbf{D}, \\ CRB_\theta^{(M)} &= \left[(\boldsymbol{\Gamma}^{(M)})^{-1} \right]_{33} = 1 / \Gamma_{33}, \\ CRB_{h_{r1}}^{(M)} &= \left[(\boldsymbol{\Gamma}^{(M)})^{-1} \right]_{44} = 1 / \Gamma_{44}, \\ CRB_{h_{11}}^{(M)} &= \left[(\boldsymbol{\Gamma}^{(M)})^{-1} \right]_{55} = 1 / \Gamma_{55}. \end{aligned} \quad (77)$$

REFERENCES

- [1] M. Heino *et al.*, "Recent advances in antenna design and interference cancellation algorithms for in-band full duplex relays," *IEEE Commun. Mag.*, vol. 53, no. 5, pp. 91–101, May 2015.
- [2] S. Hong *et al.*, "Applications of self-interference cancellation in 5G and beyond," *IEEE Commun. Mag.*, vol. 52, no. 2, pp. 114–121, Feb. 2014.
- [3] A. Sabharwal, P. Schniter, D. Guo, D. W. Bliss, S. Rangarajan, and R. Wichman, "In-band full-duplex wireless: Challenges and opportunities," *IEEE J. Sel. Areas Commun.*, vol. 32, no. 9, pp. 1637–1652, Sep. 2014.
- [4] J. Ma, G. Y. Li, J. Zhang, T. Kuze, and H. Iura, "A new coupling channel estimator for cross-talk cancellation at wireless relay stations," in *Proc. IEEE Global Telecommun. Conf. (GLOBECOM)*, Dec. 2009, pp. 1–6.
- [5] A. Masmoudi and T. Le-Ngoc, "A maximum-likelihood channel estimator for self-interference cancellation in full-duplex systems," *IEEE Trans. Veh. Technol.*, vol. 65, no. 7, pp. 5122–5132, Jul. 2016.
- [6] Y.-H. Kim and J.-H. Lee, "Channel estimation for self-interference cancellation in full-duplex wireless systems," *Wireless Pers. Commun.*, vol. 85, no. 3, pp. 1139–1152, 2015.
- [7] T. Riihonen, S. Werner, and R. Wichman, "Mitigation of loopback self-interference in full-duplex MIMO relays," *IEEE Trans. Signal Process.*, vol. 59, no. 12, pp. 5983–5993, Dec. 2011.
- [8] S. Huberman and T. Le-Ngoc, "MIMO full-duplex precoding: A joint beamforming and self-interference cancellation structure," *IEEE Trans. Wireless Commun.*, vol. 14, no. 4, pp. 2205–2217, Apr. 2015.
- [9] G. Zheng, "Joint beamforming optimization and power control for full-duplex MIMO two-way relay channel," *IEEE Trans. Signal Process.*, vol. 63, no. 3, pp. 555–566, Feb. 2015.
- [10] T. M. Kim and A. Paulraj, "Outage probability of amplify-and-forward cooperation with full duplex relay," in *Proc. IEEE Wireless Commun. Netw. Conf. (WCNC)*, Apr. 2012, pp. 75–79.
- [11] M. Duarte, C. Dick, and A. Sabharwal, "Experiment-driven characterization of full-duplex wireless systems," *IEEE Trans. Wireless Commun.*, vol. 11, no. 12, pp. 4296–4307, Dec. 2012.
- [12] T. Riihonen, S. Werner, and R. Wichman, "Residual self-interference in full-duplex MIMO relays after null-space projection and cancellation," in *Proc. Conf. Rec. 44th Asilomar Conf. Signals, Syst. Comput. (ASILOMAR)*, Nov. 2010, pp. 653–657.
- [13] X. Xiong, X. Wang, T. Riihonen, and X. You, "Channel estimation for full-duplex relay systems with large-scale antenna arrays," *IEEE Trans. Wireless Commun.*, vol. 15, no. 10, pp. 6925–6938, Oct. 2016.
- [14] L. J. Rodríguez, N. H. Tran, and T. Le-Ngoc, "Performance of full-duplex AF relaying in the presence of residual self-interference," *IEEE J. Sel. Areas Commun.*, vol. 32, no. 9, pp. 1752–1764, Sep. 2014.
- [15] L. J. Rodríguez, N. H. Tran, and T. Le-Ngoc, "Optimal power allocation and capacity of full-duplex AF relaying under residual self-interference," *IEEE Wireless Commun. Lett.*, vol. 3, no. 2, pp. 233–236, Apr. 2014.
- [16] X. Li and C. Tepedelenlioğlu, "Maximum likelihood channel estimation for residual self-interference cancellation in full duplex relay," in *Proc. Conf. Rec. 49th Asilomar Conf. Signals, Syst. Comput. (ASILOMAR)*, Nov. 2015, pp. 807–811.
- [17] X. Cheng, B. Yu, X. Cheng, and L. Yang, "Two-way full-duplex amplify-and-forward relaying," in *Proc. IEEE Military Commun. Conf. (MILCOMX)*, Nov. 2013, pp. 1–6.
- [18] F. S. Tatababa, P. Sadeghi, C. Hucher, and M. R. Pakravan, "Impact of channel estimation errors and power allocation on analog network coding and routing in two-way relaying," *IEEE Trans. Veh. Technol.*, vol. 61, no. 7, pp. 3223–3239, Sep. 2012.
- [19] D. Kim, H. Ju, S. Park, and D. Hong, "Effects of channel estimation error on full-duplex two-way networks," *IEEE Trans. Veh. Technol.*, vol. 62, no. 9, pp. 4666–4672, Sep. 2013.
- [20] F. Gao, R. Zhang, and Y.-C. Liang, "Optimal channel estimation and training design for two-way relay networks," *IEEE Trans. Commun.*, vol. 57, no. 10, pp. 3024–3033, Oct. 2009.
- [21] X. Li, C. Tepedelenlioğlu, and H. Senol, "Optimal power allocation between training and data for MIMO two-way relay channels," *IEEE Commun. Lett.*, vol. 19, no. 11, pp. 1941–1944, Nov. 2015.
- [22] J. Nocedal and S. Wright, *Numerical Optimization*. New York, NY, USA: Springer, 2006.
- [23] S. Chang and B. Kelley, "An efficient time synchronization scheme for broadband two-way relaying networks based on physical-layer network coding," *IEEE Commun. Lett.*, vol. 16, no. 9, pp. 1416–1419, Sep. 2012.
- [24] T. Riihonen, S. Werner, and R. Wichman, "Optimized gain control for single-frequency relaying with loop interference," *IEEE Trans. Wireless Commun.*, vol. 8, no. 6, pp. 2801–2806, Jun. 2009.
- [25] F. Gao, R. Zhang, and Y. C. Liang, "Channel estimation for OFDM modulated two-way relay networks," *IEEE Trans. Signal Process.*, vol. 57, no. 11, pp. 4443–4455, Nov. 2009.

- [26] K. P. Murphy, *Machine Learning: A Probabilistic Perspective*. Cambridge, MA, USA: MIT Press, 2012.
- [27] S. M. Kay, *Fundamentals of Statistical Signal Processing: Estimation Theory*. Englewood Cliffs, NJ, USA: Prentice-Hall, 1993.
- [28] U. Grenander and G. Szegö, *Toeplitz Forms and Their Applications*, vol. 321. Berkeley, CA, USA: Univ. California Press, 2001.
- [29] R. M. Gray, *Toeplitz and Circulant Matrices: A Review*. LP Breda, The Netherlands: Now Publishers, 2006.



Xiaofeng Li received the B.S. and M.S. degrees in electronic engineering from the Beijing Institute of Technology, Beijing, China, in 2009 and 2012, respectively. He is currently pursuing the Ph.D. degree in electrical engineering from Arizona State University, Tempe, AZ, USA. His research interests include channel estimation, full duplex relays, and massive MIMO.



Cihan Tepedelenlioglu (S'97–M'01) was born in Ankara, Turkey, in 1973. He received the B.S. degree (Hons.) in electrical engineering from the Florida Institute of Technology, Melbourne, FL, USA, in 1995, the M.S. degree from the University of Virginia, Charlottesville, VA, USA, in 1998, and the Ph.D. degree in electrical and computer engineering from the University of Minnesota, Minneapolis MN, USA.

From 1999 to 2001, he was a Research Assistant with the University of Minnesota. He is currently an Associate Professor of Electrical Engineering with Arizona State University, Tempe AZ, USA. His research interests include statistical signal processing, system identification, wireless communications, estimation and equalization algorithms for wireless systems, multiple-antenna communications, filter banks and multi rate systems, OFDM, ultra-wide-band systems, distributed detection, and estimation. He received the National Science Foundation (early) Career Grant in 2001.

Dr. Tepedelenlioglu has served as an Associate Editor for several IEEE transactions, including the IEEE TRANSACTIONS ON COMMUNICATIONS and the IEEE SIGNAL PROCESSING LETTERS.



Habib Şenol (S'04–M'07) received the B.Sc. and M.Sc. degrees in electronics engineering from Istanbul University, Istanbul, Turkey, in 1993 and 1999, respectively, and the Ph.D. degree in electronics engineering from Işık University, Istanbul, in 2006. He is currently an Associate Professor with the Department of Computer Engineering, Kadir Has University, Istanbul. He spent the academic year 2007–2008 with the Department of Electrical Engineering, Arizona State University, Tempe, AZ, USA, where he was involved in channel estimation and

power optimization algorithms for wireless sensor networks.

His recent research interests include communication theory, advanced signal processing techniques and their applications to wireless electrical, underwater acoustic, and optical communications.